RAA 2019 Vol. **19** No. **1**, 5(14pp) doi: 10.1088/1674–4527/19/1/5

http://www.raa-journal.org *http://iopscience.iop.org/raa*

***R**esearch in*
***A**stronomy and*
***A**strophysics*

Is the enhancement of type II radio bursts during CME interactions related to the associated solar energetic particle event?

Liu-Guan Ding[1,2], Zhi-Wei Wang[2], Li Feng[3], Gang Li[4] and Yong Jiang[2]

[1] School of Physics and Optoelectronic Engineering, Nanjing University of Information Science and Technology, Nanjing 210044, China; *dlg@nuist.edu.cn*
[2] Institute of Space Weather, Nanjing University of Information Science and Technology, Nanjing 210044, China
[3] Key Laboratory of Dark Matter and Space Astronomy, Purple Mountain Observatory, Chinese Academy of Sciences, Nanjing 210008, China
[4] Department of Space Science and CSPAR, University of Alabama in Huntsville, AL, 35899, USA

Received 2018 July 7; accepted 2018 July 27

Abstract We investigated 64 pairs of interacting-CME events identified from simultaneous observations by the *SOHO* and *STEREO* spacecraft from January 2010 to August 2014, to examine the relationship between large SEP events in the energy range of ∼25 to ∼60 MeV and properties of the interacting CMEs. We found that during CME interactions, the large SEP events in this study were all generated by CMEs with the presence of enhanced type II radio bursts, which also have wider longitudinal distributions compared to events without a type II radio burst or its enhancement (almost always associated with small SEP events). It seems that the signature of type II radio burst enhancement is a good discriminator between large SEP and small or no SEP event producers during CME interactions. The type II radio burst enhancement is more likely to be generated by CME interactions, with the main CME having a larger speed (v), angular width (WD), mass (m) and kinetic energy (E_k), and taking over the preceding CMEs. The preceding CMEs in these instances have higher v, WD, m and E_k than those in CME pairs missing type II radio bursts or enhancements. Generally, the values of these properties in the type-II-enhanced events are typically higher than the corresponding non-type-II or non-type-II-enhanced cases for both the main and preceding CMEs. Our analysis also revealed that the intensities of associated SEP events correlate negatively with the intersection height of the two CMEs. Moreover, the overlap width of two CMEs is typically larger in type-II-enhanced events than in non-type-II or non-type-II-enhanced events. Most type-II-enhanced events and SEP events are coincident and are almost always made by the fast and wide main CMEs that sweep fully over relatively slower and narrower preceding CMEs. We suggest that a fast CME with enough energy completely overtaking a relatively narrower preceding CME, especially at low height, can drive a more energetic shock signified by the enhanced type II radio bursts. The shock may accelerate ambient particles (likely provided by the preceding CME) and lead to large SEP events more easily.

Key words: Sun: coronal mass ejections (CMEs) — Sun: radio radiation — Sun: particle emission — Sun: CME interaction

1 INTRODUCTION

Solar energetic particles (SEPs) are a serious radiation hazard for spacecraft and astronauts in space. The relationship between SEP and solar activities is also a central topic in space physics and space weather. SEP events are usually classified into two types according to their different acceleration processes: impulsive and gradual events, thought to be produced by solar flare and coronal mass ejection (CME)-driven shocks respectively (Reames 1995, 1999). Gradual SEP events usually present distinctive features compared to impulsive events, such as high peak flux intensity, high energy, long duration, etc. (e.g. Reames 1995, 1999; Kahler 1996, 2005). However, in many cases (e.g. Cane & Richardson 2003; Li et al. 2007a,b; Ding et al. 2016), gradual and impulsive SEP components are mixed

and cannot be distinctively classified into these two types. So, the solar source of energetic particles in large SEP events is still a popular issue. Some statistical results implied that more energetic particles (e.g. $> 30\,\mathrm{MeV}$) are dominantly accelerated by concurrent solar flares, while CME-driven shocks are generally an effective accelerator mainly for SEPs with lower energies (e.g. Le et al. 2017; Le & Zhang 2017). The spectral rigidity of ground level enhancement (GLE) also revealed that flares play an important role in large gradual SEP events (Wu & Qin 2018). The case study presents evidence that the first arriving relativistic and non-relativistic protons and electrons are accelerated by the concurrent flare according to timing analysis in an individual SEP event, and then these particles may be further accelerated by the associated CME-driven shock (Zhao et al. 2018).

In general, large SEP events, e.g. $I_{\mathrm{p}}\ >10\,\mathrm{pfu}$ (pfu = proton $\mathrm{cm}^{-2}\,\mathrm{s}^{-1}\,\mathrm{sr}^{-1}$) at $>10\,\mathrm{MeV}$ in *GOES* observations are almost always associated with fast and wide CME eruptions, but inversely not all fast and wide CMEs can produce SEP events. So, a number of mechanisms for CMEs generating SEPs have been proposed, such as coronal waves, CME lateral expansion, CME-CME interaction and so on (Desai & Giacalone 2016; Lugaz et al. 2017).

The intensity of a large gradual SEP event is positively correlated with the speed of the associated CME, but the scatter is very large (Kahler 1996; Kahler et al. 2000). This suggested that the number of ambient energetic particles may be another factor determining the intensity of the associated SEP event in addition to the associated CME-driven shock speed (e.g Kahler 2001; Kahler & Vourlidas 2014). These seed particles may be from solar flares (Mason et al. 1999, 2000) or from the preceding CMEs (Gopalswamy et al. 2002, 2004; Li et al. 2012).

CME interaction is a frequent phenomenon in the solar corona and interplanetary (IP) space. Usually CME "cannibalism" or collision can happen in the process of two interacting CMEs (e.g. Gopalswamy et al. 2001; Temmer et al. 2014; Shanmugaraju et al. 2014). Shen et al. (2012) presented a case of two CMEs colliding in IP space and revealed that these two magnetized plasmoids collided as if they were solid-like objects, with a likelihood of 73% that the collision was super-elastic. In a study of the first GLE event of solar cycle 24, which occurred on 2012 May 17, Shen et al. (2013b) reported two CMEs erupting from a complicated active region separated by only 3 minutes using observations from *STEREO* and *SOHO*. Successive CMEs can also cause an extreme space weather storm in IP space via interaction and pre-conditioning of the IP medium at the CMEs (Liu et al. 2014). Gopalswamy et al. (2002, 2003) suggested that CME interaction is an important aspect of SEP production, which can act as a good discriminator between SEP-poor and SEP-rich CMEs. However, Richardson et al. (2003) argued that this interaction does not play a fundamental role in determining whether a wide and fast CME is associated with an SEP event.

Gopalswamy et al. (2004) showed that a strong correlation exists between high particle intensities and the presence of preceding CMEs within 24 hours. The interpretation is that seed particles may be trapped in closed field lines of the preceding CMEs or associated turbulence so that they are subject to repeated acceleration by the shock driven by the second CME. However, this time interval between two CME eruptions is too long to ensure that direct CME (shock)-CME interaction is responsible for the observed large SEP events, because most large SEPs are believed to occur below $\sim 10\,R_{\mathrm{s}}$ (R_{s} is the solar radius) (Kahler 2003). Later, Li & Ma (2005) suggested that two consecutive CMEs may provide a favorable environment for particle acceleration. Subsequently, Li et al. (2012) proposed the "twin-CME" scenario, where two CMEs erupt in sequence from the same or nearby active regions within a short period of time. The preceding CME or its shock can increase the turbulence level and/or seed population ahead of the main CME-driven shock. Thereby, the enhanced turbulence level and seed population favor a more efficient particle acceleration at the main CME shock compared to a single CME. Ding et al. (2013) extended the work of Li et al. (2012) and found that CMEs having a preceding CME with speed $> 300\,\mathrm{km\,s}^{-1}$ within 9 hours from the same active region have a larger probability of leading to large SEP events than CMEs that do not have preceding CMEs. A subsequent case study showed that the SEP release time near the Sun is consistent with the time of the main CME leading edge overtaking the trailing edge of the preceding CME, as well as the radio enhancement (Ding et al. 2014b).

Type II radio bursts have often been used as a diagnostic for a CME-driven shock in studying SEP events (e.g. Kahler 1982; Gopalswamy et al. 2005; Cho et al. 2008). Metric type II radio bursts are generated when the shock is close to the Sun (e.g. $\leq 3\,R_{\mathrm{s}}$) (Gopalswamy et al. 2009). While many SEP events have metric type II bursts associated with them, the signature of metric type II bursts does not necessarily lead to a large SEP event (Kahler 1982). Cliver et al. (2004) argued that the presence of decahectometric (DH) type II radio emissions may be used as a marker to distinguish between SEP-rich and SEP-poor metric type II radio bursts. Later, Gopalswamy et al. (2005)

found that CMEs tend to be more energetic if radio bursts appear from metric to DH wavelengths. Usually, a shock that survives beyond $3\,R_{\rm s}$, indicated by the signature of type II radio emission from metric drifting to DH wavelengths, is stronger and broader (e.g. Cliver et al. 2004).

CME interaction can lead to radio enhancement following an IP type II burst when a fast CME overtakes a slow one, which may imply a strengthened shock (Gopalswamy et al. 2001) (also see Shen et al. 2013b; Ding et al. 2014b; Temmer et al. 2014). The result of Temmer et al. (2014) indicated that the interaction process is strongly position angle dependent in terms of timing as well as kinematical evolution and the timing of enhanced type II bursts may be related to shock streamer interaction.

In previous statistical works on CME interaction and its role in SEP production by, e.g., Gopalswamy et al. (2002, 2003, 2004); Ding et al. (2013), the observations of CMEs and SEPs were all only made by spacecraft near the Earth. However, the CME projection effect and the longitudinal dependence of SEP flux detection are always inevitable, especially in the study of CME interaction. In this paper, we make use of observations by multiple spacecraft and focus on the effect of CME interactions on the association with SEP events and radio enhancement by using *SOHO* and *STEREO-A*/*B* (*STA*/*STB*) data. *STA* and *STB* spacecraft are advancing ahead of or lagging behind Earth at $\sim$ 1 AU in heliocentric orbits respectively, and separating slowly from the Earth by $\sim$ 22° year^{-1}. During the study period from January 2010 to August 2014, the separation between *STA*(*B*) and Earth increased from $\sim 64°(68°)$ to $\sim 166°(161°)$. Our paper is organized as follows: Section 2 presents the dataset; Section 3 shows our statistical results; and Section 4 contains the discussion and conclusions.

2 DATASET AND ANALYSIS

From the online CME catalog CDAW (*https://cdaw.gsfc.nasa.gov/CME_list/*), we identified 64 interacting CME pairs from January 2010 to August 2014 which satisfied the following criteria:

(1) The time interval between the main and preceding CMEs is less than 14 hours (Ding et al. 2014a).
(2) The angular width (WD) of both the main CME (fast one) and the preceding CME (pre-CME, slow one) is larger than 60°, ensuring that these two CMEs can be clearly identified simultaneously by *SOHO*/LASCO (Brueckner et al. 1995) and *STEREO*/SECCHI (Howard et al. 2008) images.
(3) The main CME can overtake the preceding CME within the field of view (FOV) of both *SOHO*/LASCO C2-C3 and *STEREO*/SECCHI COR1-COR2 instruments (i.e. height $\leq\sim 30\,R_{\rm s}$). This criterion removes false interaction due to the projection effect from a single view point.
(4) The angular span area of the preceding CME needs to intersect partly or fully with the main CME to ensure the interaction. We note that the dataset of this study is a subset of the twin-CME database introduced in Ding et al. (2013).

The properties of main CMEs and preceding CMEs are listed in Table 1, which are taken from the CDAW online database. Column (1) is the event number; column (2) is the onset time (first appearance in LASCO/C2) of the main (preceding) CME; column (3) is the central position angle (CPA); column (4) is the WD; column (5) is the CME speed (v) projected to the sky plane from the perspective at Earth; columns (6) and (7) are the mass (m) and kinetic energy (E_k) respectively. Columns (8) to (13) list similar parameters for the preceding CME. By using a quadratic polynomial fit to height-time measurements of the CMEs at CDAW, the intersection heights of leading-edge trajectories for the main and preceding CME are obtained, which are listed in Column (14) of Table 1 (and labeled as $H_{\rm int}$).

Type II radio bursts yield information on the formation and propagation of the CME associated shock. For example, Figure 1 shows the dynamic spectra of the events on 2014 August 25 and 2014 August 28 within DH wavelengths, detected by *Wind*/WAVES and *STB*/SWAVES respectively. The features of frequency shift, indicated by the arrows, are distinct. Note, however, the type II radio intensities in panel (a) are weaker and those in (b) are stronger. A continuum-like enhancement of decametric to hectometric type II radio emission is present in low frequency for the event in panel (b) (indicated by a box), which may be interpreted as the observational signature of transit of the shock front for a fast CME through the core of a slow CME as a consequence of CME interactions (also see Gopalswamy et al. (2001)). This unusually enhanced spectral continuum in DH wavelengths is the main subject of this paper and is defined as enhanced type II radio bursts or type II radio enhancement. So in Figure 1, the event in panel (a) is associated with a type II radio burst but no enhancement, while the event in panel (b) is associated with an enhanced type II radio burst. To ensure that the type II radio enhancement indeed corresponds to the interaction, we compare the time of trajectory intersection to the time of enhancement. Only when the intersection time (e.g. indicated by the dot-dot-dot-dashed lines in Fig. 1) is later than the start time of radio burst enhancement, which means the enhancement has occurred during the main CME transiting through the body

Table 1 The Properties of Two Interacting CMEs (2010–2014)

No.	Main CME						Preceding CME						$H_{\rm int}$[a]	type II[b]	type II enhan.	$I_{\rm ps}$	$I_{\rm pa}$	$P_{\rm pb}$
	Onset time	CPA	WD	v	m	E_k	Onset time	CPA	WD	v	m	E_k						
		(°)		(km s^{-1})	(g)	(erg)		(°)		(km s^{-1})	(g)	(erg)	(Rs)			(cm^{-2} s^{-1} sr^{-1})		(MeV^{-1})
(1)	(2)	(3)	(4)	(5)	(6)	(7)	(8)	(9)	(10)	(11)	(12)	(13)	(14)	(15)	(16)	(17)	(18)	(19)
1	2010/02/13 23:18	290	63	1005	2.7e+15	1.3e+31	2010/02/13 19:54	290	126	247	4.5e+15	1.4e+30	3.6	–	N	–	–	–
2	2010/03/17 12:30	259	66	870	8.5e+14	3.2e+30	2010/03/16 22:30	229	76	113	2.2e+15	1.4e+29	12.0	–	N	–	–	–
3	2010/08/18 05:48	255	184	1471	1.1e+16	1.2e+32	2010/08/18 00:24	298	88	403	7.6e+15	6.1e+30	16.7	DH	N	0.0076	0.0057	0.0013
4	2011/02/01 23:24	276	360	437	1.5e+15	1.4e+30	2011/02/01 20:00	288	77	79	3.1e+14	9.6e+27	4.5	–	N	–	–	–
5	2011/02/24 07:48	70	158	1186	7.5e+15	5.3e+31	2011/02/24 02:36	56	71	146	2.8e+13	3.0e+27	7.0	M	N	–	–	–
6	2011/04/17 01:25	46	75	218	5.6e+14	1.3e+29	2011/04/17 00:00	359	96	179	2.4e+15	3.8e+29	3.5	–	N	–	–	–
7	2011/05/09 20:57	55	292	1318	1.0e+16	8.8e+31	2011/05/09 07:36	58	98	132	6.3e+15	5.5e+29	13.3	DH	Y	–	–	0.0016
8	2011/05/12 13:25	33	95	274	5.4e+14	2.0e+29	2011/05/12 08:36	130	110	166	4.0e+15	5.5e+29	4.3	–	N	–	–	–
9	2011/06/02 08:12	99	360	976	1.4e+15	6.8e+30	2011/06/02 07:24	74	61	253	1.4e+14	4.4e+28	3.5	DH	N	–	–	–
10	2011/09/06 23:05	306	360	575	1.5e+16	2.5e+31	2011/09/06 21:24	289	115	499	9.7e+15	1.2e+31	21.1	DH	Y	0.0663	–	0.0048
11	2011/10/04 13:25	379	360	1101	1.6e+16	9.9e+31	2011/10/04 12:12	30	124	393	6.2e+14	4.8e+29	4.8	DH	Y	–	0.0162	0.1155
12	2011/10/14 12:24	32	241	814	7.9e+15	2.6e+31	2011/10/14 09:12	40	208	454	1.1e+16	1.1e+31	19.6	DH	N	–	–	–
13	2011/10/20 03:36	298	193	893	4.6e+15	1.8e+31	2011/10/19 21:48	302	60	239	2.4e+15	6.8e+29	11.8	–	N	–	–	–
14	2011/10/22 01:25	313	360	593	1.6e+16	2.7e+31	2011/10/21 17:48	242	96	292	1.1e+16	4.7e+30	27.1	–	N	–	–	–
15	2011/11/07 23:48	303	109	527	3.2e+15	4.4e+30	2011/11/07 20:57	280	82	305	9.8e+14	4.6e+29	10.5	–	N	–	–	–
16	2011/11/09 13:36	62	360	907	1.4e+16	5.6e+31	2011/11/09 08:36	132	147	496	1.3e+16	1.6e+31	29.2	M,DH	Y	–	–	0.0027
17	2011/11/26 07:12	277	360	933	1.2e+16	5.2e+31	2011/11/26 00:36	250	90	292	7.4e+15	3.2e+30	17.9	DH	Y	0.1017	0.0066	0.0020
18	2011/12/09 12:12	74	117	335	9.7e+14	5.4e+29	2011/12/09 05:36	163	83	155	7.2e+14	8.7e+28	11.9	–	N	–	–	–
19	2011/12/24 00:36	56	61	475	2.8e+15	3.1e+30	2011/12/23 18:36	104	74	247	2.2e+15	6.9e+29	14.1	–	N	–	–	–
20	2012/01/12 08:24	69	360	814	1.0e+16	3.4e+31	2012/01/12 04:24	79	101	280	3.7e+15	1.4e+30	11.3	DH	N	–	–	–
21	2012/01/19 14:36	19	360	1120	1.9e+16	1.2e+32	2012/01/19 09:48	333	111	317	9.9e+15	5.0e+30	13.7	DH	N	–	–	0.0197
22	2012/01/23 04:00	302	360	2175	2.6e+16	6.2e+32	2012/01/23 03:12	329	221	684	5.3e+15	1.2e+31	6.6	DH	Y	10.3404	0.2319	0.4717
23	2012/03/04 11:00	52	360	1306	7.9e+15	6.8e+31	2012/03/04 08:12	61	92	207	–	–	5.6	M,DH	Y	0.0026	–	0.2263
24	2012/03/05 04:00	391	360	1531	1.4e+16	1.6e+32	2012/03/05 03:12	29	92	594	3.5e+15	6.2e+30	5.9	DH	Y	0.0085	–	0.1901
25	2012/03/10 18:00	276	360	1296	–	–	2012/03/10 16:24	292	127	423	4.3e+15	3.8e+30	8.0	M,DH	Y	–	–	–
26	2012/03/18 00:24	303	360	1210	1.1e+16	7.9e+31	2012/03/17 22:12	348	64	66	7.9e+14	1.7e+28	3.7	–	N	–	–	–
27	2012/03/28 01:36	397	360	1033	7.0e+15	3.8e+31	2012/03/28 00:48	60	126	664	–	–	12.6	–	N	–	–	–
28	2012/04/16 17:48	62	166	1348	7.3e+15	6.7e+31	2012/04/16 14:12	55	134	89	2.0e+15	7.9e+28	4.3	–	N	–	–	–
29	2012/06/28 20:00	42	145	1313	7.3e+15	6.3e+31	2012/06/28 18:48	127	83	343	2.4e+15	1.4e+30	4.9	DH	N	–	–	–
30	2012/07/17 13:48	255	176	958	1.7e+16	7.8e+31	2012/07/17 13:25	153	95	292	4.4e+15	1.9e+30	5.2	M,DH	Y	0.4160	–	–
31	2012/08/04 13:36	109	360	856	1.3e+16	4.7e+31	2012/08/04 12:36	124	60	187	1.5e+15	2.6e+29	4.0	–	N	–	–	–
32	2012/08/10 10:34	230	251	464	6.7e+15	7.2e+30	2012/08/10 00:44	319	92	188	4.7e+15	8.2e+29	19.9	–	N	0.0007	0.0045	–
33	2012/08/18 00:48	62	145	986	3.6e+15	1.8e+31	2012/08/17 23:48	338	185	463	5.4e+15	5.7e+30	7.8	–	N	–	–	–
34	2012/08/20 21:28	68	360	521	7.5e+15	1.0e+31	2012/08/20 19:36	35	75	215	1.5e+14	3.5e+28	5.8	–	N	–	–	–
35	2012/08/26 11:12	330	143	398	1.2e+15	9.6e+29	2012/08/26 07:24	25	86	208	1.9e+15	4.0e+29	6.7	–	N	–	–	–
36	2013/02/14 21:17	274	81	690	6.6e+15	1.6e+31	2013/02/14 19:24	273	60	200	2.0e+15	3.9e+29	5.6	–	N	–	–	–
37	2013/03/05 03:48	424	360	1316	1.9e+16	1.7e+32	2013/03/05 00:36	90	81	80	2.4e+15	7.8e+28	3.9	M,DH	Y	0.0024	11.0666	0.1183
38	2013/03/24 15:48	265	73	491	8.0e+14	9.7e+29	2013/03/24 07:48	335	62	180	1.9e+15	3.1e+29	7.0	–	N	–	–	–
39	2013/04/20 06:00	283	153	741	1.1e+16	3.0e+31	2013/04/20 03:48	284	73	133	1.4e+15	1.3e+29	5.0	–	N	–	–	–
40	2013/04/26 22:00	256	67	561	2.8e+15	4.4e+30	2013/04/26 18:24	200	150	271	5.7e+15	2.1e+30	5.8	–	N	–	–	–
41	2013/05/17 09:12	74	360	1345	5.8e+15	5.2e+31	2013/05/17 04:49	78	86	107	1.5e+15	8.4e+28	5.0	M	N	–	–	–
42	2013/05/22 13:25	251	360	1466	3.3e+16	3.5e+32	2013/05/22 08:48	270	210	687	3.1e+16	7.3e+31	6.4[c]	M,DH	Y	8.2122	0.0355	–
43	2013/07/01 20:24	123	208	819	1.3e+16	4.5e+31	2013/07/01 08:12	7	98	71	3.1e+15	7.7e+28	7.3	–	N	–	0.0018	0.0056
44	2013/07/06 19:36	147	123	380	2.7e+15	1.9e+30	2013/07/06 12:36	101	236	127	9.0e+14	7.2e+28	16.1	–	N	–	–	–
45	2013/07/18 20:24	102	63	939	4.1e+15	1.8e+31	2013/07/18 18:24	102	135	458	4.9e+15	5.2e+30	11.0	–	N	–	–	–
46	2013/07/29 13:25	42	145	542	2.9e+15	4.2e+30	2013/07/29 10:36	155	124	226	1.7e+15	4.4e+29	7.3	–	N	–	–	–
47	2013/10/11 07:24	88	360	1200	1.0e+16	7.3e+31	2013/10/11 01:36	21	108	269	4.9e+15	1.8e+30	11.5	M,DH	Y	0.0011	2.1588	0.2092
48	2013/10/24 01:25	122	360	399	1.9e+15	1.5e+30	2013/10/23 23:12	93	110	162	1.3e+15	1.7e+29	4.8	M	N	–	–	–
49	2013/10/28 04:48	315	156	1201	6.3e+15	4.5e+31	2013/10/28 02:24	265	360	695	8.6e+15	2.1e+31	26.1	DH	Y	0.0143	0.0031	–
50	2013/12/26 03:24	130	360	1336	5.6e+15	5.0e+31	2013/12/26 03:12	122	171	1022	9.4e+15	4.9e+31	8.7	DH	Y	0.0107	0.2317	0.1907
51	2014/01/06 00:36	276	129	574	1.9e+15	3.2e+30	2014/01/05 19:00	301	101	269	2.5e+15	9.1e+29	17.3	–	N	–	–	–
52	2014/01/16 23:36	114	197	666	1.1e+16	2.5e+31	2014/01/16 21:38	95	113	438	2.1e+15	2.0e+30	11.6	–	N	–	–	–
53	2014/01/25 16:48	152	158	783	2.5e+15	7.8e+30	2014/01/25 14:48	127	80	299	4.8e+14	2.1e+29	7.3	–	N	–	–	–
54	2014/01/30 16:24	120	360	1087	1.0e+16	6.0e+31	2014/01/30 15:48	109	62	780	3.0e+15	9.3e+30	7.1	M	N	0.0008	–	–
55	2014/01/30 08:24	117	360	458	4.5e+15	4.7e+30	2014/01/30 06:12	64	75	116	1.1e+14	7.6e+27	4.1	–	N	–	–	–
56	2014/02/21 16:00	86	360	1252	7.2e+15	5.6e+31	2014/02/21 12:12	184	62	341	8.4e+14	4.9e+29	11.3	DH	N	–	0.0038	0.0472
57	2014/03/14 03:24	58	66	314	1.7e+15	8.5e+29	2014/03/14 01:36	133	91	110	1.4e+15	8.4e+28	4.2	–	N	–	–	–
58	2014/03/22 10:00	323	169	756	5.9e+15	1.7e+31	2014/03/22 06:48	257	168	340	7.8e+15	4.5e+30	10.0	–	N	–	–	–
59	2014/04/05 00:12	155	149	585	4.0e+15	6.8e+30	2014/04/04 21:12	58	73	359	5.9e+14	3.8e+29	8.4	–	N	0.0025	–	–
60	2014/05/09 02:48	276	360	1099	1.3e+16	7.7e+31	2014/05/09 01:25	236	92	161	1.8e+15	2.4e+29	6.6	DH	Y	0.0020	–	–
61	2014/07/20 03:12	72	135	417	5.2e+15	4.6e+30	2014/07/19 20:12	62	76	135	1.8e+15	1.7e+29	11.0	–	N	–	–	–
62	2014/07/30 16:12	139	143	638	4.4e+15	8.9e+30	2014/07/30 13:36	41	124	274	4.0e+15	1.5e+30	7.0	–	N	–	–	–
63	2014/08/25 15:36	272	360	555	–	–	2014/08/25 13:48	252	75	315	3.9e+14	1.9e+29	8.4	M,DH	N	0.0053	–	–
64	2014/08/28 17:24	415	360	766	1.0e+16	2.9e+31	2014/08/28 11:48	13	93	190	3.7e+15	6.7e+29	10.4	DH	Y	0.0005	0.1472	0.1781

Notes: *a* The intersection height of leading-edge trajectories for two CMEs. A quadratic fitting is used for the relationship between CME height and time. *b* Type II radio bursts associated with the main CME. M – metric type II radio burst observed by ground stations, such as Learmonth, Palehua, San-vito or Sagamore-hill; DH – DH type II radio burst observed by *Wind*/WAVES or *STEREO*/SWAVES. '–' denotes no type II radio burst. *c* This value is cited from (Ding et al. 2014b).

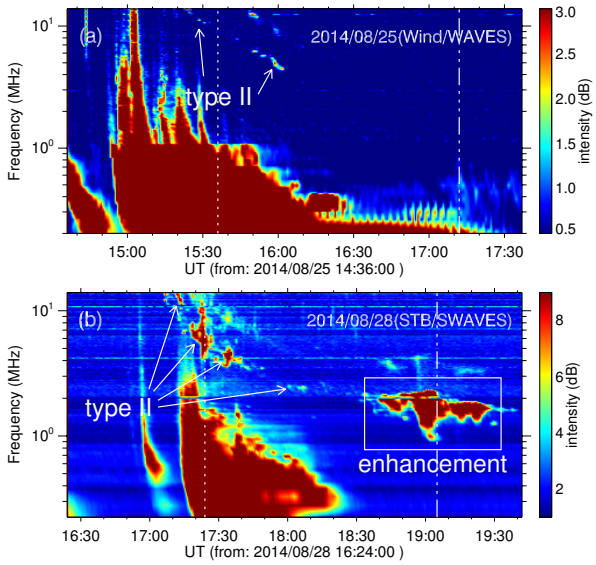

Fig. 1 A couple of examples displaying the type II radio bursts without (a) or with (b) enhancement during CME interactions. The *dotted line* indicates the onset time of the associated CME in the LASCO C2 FOV, and the *dot-dot-dot-dashed line* represents the intersection time for leading-edge trajectories of the main CME crossing the pre-CME.

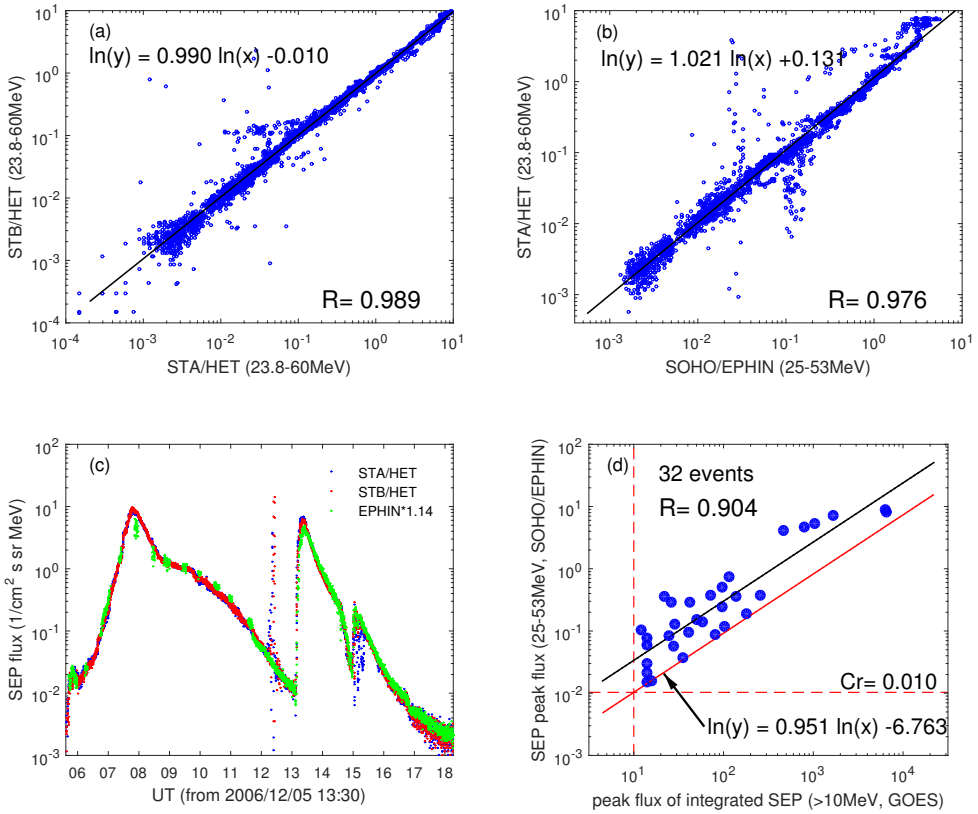

Fig. 2 Comparison of the differential solar energetic proton intensities in *STEREO*/HET and *SOHO*/EPHIN using observations during December 2006, and the peak intensity of SEP events from 2010 to 2014 between *SOHO*/EPHIN and *GOES*. (a) *STB*/HET vs. *STA*/HET in 23.8–60 MeV; (b) *STA*/HET in 23.8–60 MeV vs. *SOHO*/EPHIN in 25–53 MeV; (c) energetic proton flux time profiles in *STA* 23.8–60 MeV (*blue*), *STB* in 23.8–60 MeV (*red*) and *SOHO* in 25–53 MeV multiplied by 1.14 (*green*); (d) peak flux of proton intensity in *SOHO*/EPHIN 25–53 MeV vs. that in *GOES* $>$ 10 MeV for large SEP events. The *black lines* are the linear fits to the data; the *red solid line* indicates the lower limit of data, which is shifted from the linear fit with the same slope.

of the preceding CME, is radio enhancement considered to be associated with the CME interaction. Similar cases can also be seen from Gopalswamy et al. (2001); Ding et al. (2014b).

Type II radio bursts associated with the main CMEs are listed in Column (15). 'M' denotes the metric type II radio burst detected by ground stations, such as Learmonth, Palehua, San-vito and Sagamore-hill *(https://www.ngdc.noaa.gov/stp/space-weather/solar-data/solar-features/solar-radio)*. 'DH' denotes the DH type II radio burst observed by *Wind*/WAVES *(ftp://cdaweb.gsfc.nasa.gov/pub/data/wind/waves)* (Bougeret et al. 1995) and/or *STA*(*B*)/SWAVES *(ftp://stereoftp.nascom.nasa.gov/pub/ins_data/swaves)* (Bougeret et al. 2008). Column (16) indicates whether the type II radio burst enhancement is due to the interaction of two CMEs (Y-yes or N-no).

During the *STEREO* era, SEP observations were made from multiple locations at 1 AU and observations of the far side of the Sun were available, allowing the far side sources of SEPs to be identified (Lario et al. 2013; Richardson et al. 2014). This leads to a great advantage over single-point observations. For single point observation, the quality of magnetic connection between the source location and the spacecraft often decides the flux level of an event and therefore if the event can be classified as an SEP. This is particularly true for backside events and small events (Reames et al. 1996). For multi-spacecraft events, we can construct better criteria to identify cases as large SEP events. In this work, we use the energetic particle observations made by the HET instrument onboard *STA*/*B* (von Rosenvinge et al. 2008) and the EPHIN instrument onboard *SOHO* (Müller-Mellin et al. 1995). For *STEREO*, we focus on the energy range 23.8–60 MeV, defined by a combination of HET energy channels, to enhance the count statistics. For *SOHO*, we use the energy range 25–53 MeV of the EPHIN instrument, which matches 23.8–60 MeV on *STEREO*/HET. The intercalibration between the various instruments used in this study can be checked over a wide dynamic range during the events in December 2006, when the *STEREO* spacecraft were still close to the Earth (e.g. Lario et al. 2013; Richardson et al. 2014). Figure 2 shows the results of comparison between different instruments in the energy range above. The black solid lines are the linear fits to the data. Figure 2(a) displays five minute average proton intensity from *STA*/HET plotted against *STB*/HET at the same energy range. The energetic proton intensities at both spacecraft are highly correlated ($R = 0.989$), with similar intensities (i.e. $I(B) = 0.990I(A)^{0.990}$), which suggests that the observed intensities by *STA* and *STB* are comparable. Figure 2(b) displays the 23.8–60 MeV proton intensities from *STA*/HET plotted versus the 25–53 MeV proton intensities from *SOHO*/EPHIN. The *STA*/HET intensity is correlated with $R = 0.976$, but ~ 1.14 times higher than, the *SOHO*/EPHIN intensity in a slightly narrow energy range. So in this study, the *SOHO*/EPHIN intensity is multiplied by a factor of 1.14, which can be compared with the *STEREO*/HET intensity, thus allowing us to compare intensities of SEP events measured by selected instruments onboard different spacecraft. Figure 2(c) presents the proton flux of *SOHO*/EPHIN (*1.14) and *STEREO*/HET from 2006 December 5 to 18, which shows good agreement between each other in both the ascending phases and the decaying phases of the SEP events.

The integrated proton flux detected by the *GOES* instrument is usually used to define a large SEP event (e.g. the peak flux $\geq$10 pfu at $>$10 MeV energy channel). To obtain the intensity threshold for identifying large SEP events from *STEREO*/HET and *SOHO*/EPHIN at $\sim$25 – $\sim$60 MeV, we compare the *SOHO*/EPHIN 25–53 MeV and *GOES* $>$10 MeV peak intensities of 32 large SEP events from 2010 to 2014, shown with a good correlation ($R = 0.904$) in panel (d) because of the close location of *SOHO* and *GOES* near the Earth. We then shift the linear fit line down to the lower limit of the data, indicated by the red solid line, given by an empirical formula $y = 0.00114x^{0.951}$. Using this relationship, the criterion of a large SEP event is obtained to be 0.01 (cm^{-2} s^{-1} sr^{-1} MeV^{-1}) for *SOHO*/EPHIN at 25–53 MeV. We note that a few small events using the criterion of *GOES* may become SEP events using this threshold due to implementation of the lower limit in Figure 2(d). With the multiplicative factor of 1.14 applied to *SOHO*/EPHIN observations, this value is set to 0.0114 (cm^{-2} s^{-1} sr^{-1} MeV^{-1}) hereafter. The SEP peak intensities measured by different spacecraft are listed in columns 17–19 of Table 1 respectively: $I_{\rm ps}$ – *SOHO*/EPHIN*1.14, $I_{\rm pa}$ – *STA*/HET and $I_{\rm pb}$ – *STB*/HET. The symbol '–' denotes that there was no detectable SEP event.

3 RESULTS

3.1 Type II Radio Bursts Associated with SEP Events

Type II radio bursts are generally used to indicate whether a shock is formed during the CME eruption. When the shock propagates from the low corona to high corona, the frequency of type II radio emission, decided by the ambient plasma density, decreases from metric wavelengths to DH wavelengths since the coronal plasma density de-

creases. The fast CME overtaking the preceding CME is usually accompanied by type II radio enhancement (e.g. Gopalswamy et al. 2001; Ding et al. 2014b). However, not all cases of CME interaction lead to type II radio burst or enhanced type-II radio bursts, because radio emission or its enhancement also depends on the properties of the CME pair, such as CME speed, kinetic energy, spatial relation and so on. Here, we classified all 64 CME pairs in this study into two groups: (1) cases with enhanced type II radio burst (19 events: en-type-II events); (2) cases with type-II radio burst but no enhancement or without any type II radio burst (45 events: no-en-type-II events).

For an individual SEP event, the detected peak intensity by a given spacecraft may be significantly affected by longitudinal separation between the solar source location and the footpoints of magnetic field lines connecting the spacecraft to the Sun, or the longitude of the spacecraft relative to the location of the solar event. We therefore selected the maximum value among peak intensities observed by three spacecraft (*SOHO* and *STA*/*B*) as the nominal intensity of this event (labeled by '$I_{\rm p}$' hereafter). Compared to single spacecraft observations, our method will decrease the chance of a large SEP event being missed or underestimated due to poor magnetic connection.

Among 24 SEP events listed in Table 1, 18 events (including all 15 large SEP events) are associated with CME pairs assigned to group 1, and six events (only small SEP events) to group 2. The histograms of SEP log peak intensities for two groups are shown in Figure 3(a-b, top). The colors dark red, red, green and blue indicate events that are associated with type II radio bursts in metric (M), metric-DH (M-DH), DH wavelength and no type II radio signatures, respectively. The log $I_{\rm p}$ of SEP events in group 1 varies from –2.80 to 1.04 (average –0.88, median –0.84), while $\log I_{\rm p}$ of SEP events in group 2 varies from –3.08 to –2.12 (average –2.45, median –2.31). It is clear that the intensity of the SEP event when an enhanced type II radio burst is present is larger than that when type II radio emission or its enhancement is absent. Gopalswamy et al. (2005) examined the role of metric radio bursts and DH radio bursts in large SEP events. They found that CMEs tend to be more energetic if radio bursts appear in all three wavelength ranges (i.e. from m-to-km). Since the plasma frequency at $\sim 3R_s$ is $\sim$14 MHz, Cliver et al. (2004) suggested the shocks that survive beyond $3\,R_s$ are stronger and broader, and therefore accelerate particles to high energies. From panels (a) and (b), we see clearly that the majority of SEP events associated with metric type II radio bursts (M and M-DH) in group 1 is more intense. This is not true for events in group 2. It is easily understood that a shock exhibiting metric type II radio bursts is a stronger accelerator that can produce a larger SEP event if enough seed particles from the core of the preceding CME are overtaken by the shock identified by enhancement of type II radio bursts. Panel (c) shows the percentage of en-type-II SEP events in each $I_{\rm p}$ bin, which indicates that all large SEP events (i.e. $I_{\rm p} \geq$0.0114) are from group 1. Here, one may ask which factor correlates the most significantly with SEP intensity: the presence or absence of type II emission itself or the presence or absence of enhancement of type II radio burst? From Table 1 and Figure 3, we see that: 18/19 (95%) CME pairs in which radio enhancements are present generate SEP events. In comparison, only 6/45 (13%) CME pairs in which type II radio emissions or enhancements are absent can generate SEP events. By comparison, 21/29 (72%) CME pairs with the presence of type II can lead to SEP events, and 3/35 (9%) without can lead to SEP events. If only considering large SEP events, 15/19 (79%) CME pairs with enhanced type II can produce large SEP events, while only $15/29$ (52%) CME pairs with type II can produce large SEP events. Clearly, the presence of enhancements of type II radio bursts correlates better with the occurrence of SEP and its size, compared to the presence of type II radio emission alone. So, it is suggested that, for interacting CME pairs, the majority of SEP events is generated by fast CMEs overtaking preceding CMEs and leads to type II radio enhancement, especially for large SEP events. The signature of type II radio burst enhancement during CME interactions seems to be a good discriminator between large and small or no SEP event producers.

We also examine the number of spacecraft that can observe SEP flux increasing from the background in the energy range of $\sim$25 to $\sim$60 MeV, shown in Figure 3(d-f, bottom). The number of SEP-observed spacecraft may be used roughly to indicate the longitudinal spreading of energetic particles and/or the shock strength. From panel (f), the percentage of events accompanied by enhanced type II radio bursts rises from around 63% for one-spacecraft events to around 78% for two-spacecraft events, and around 86% for three-spacecraft events. This could be a selection effect in that the shocks are more intense when type II radio enhancements are present during the CME interactions.

3.2 Properties of en-type-II and no-en-type-II Interacting CMEs

Since type II radio burst enhancement can serve as a distinct signature of occurrence of a large SEP event during the interaction of CME pairs, what properties of the main

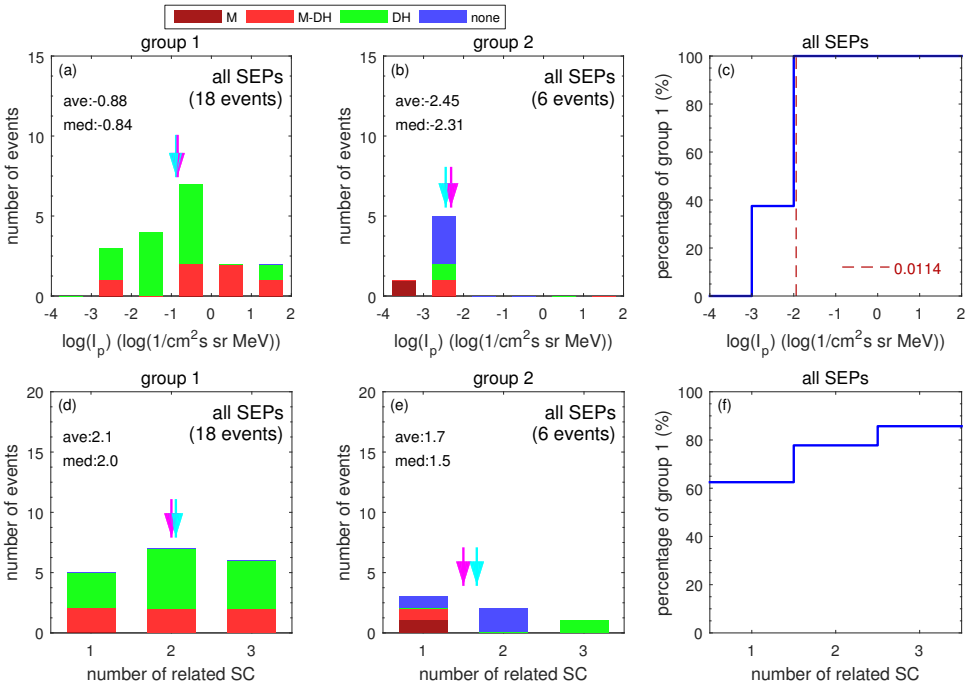

Fig. 3 Histograms of the intensities ($I_{\rm p}$) of SEP events associated with the two CMEs interacting are shown in panels (a,b). Histograms of the number of different spacecraft that detected the same SEP event are shown in panels (d,e). In each bar, *dull red*, *red* and *green* colors indicate the events that are associated with type II radio bursts emitted in metric (M) wavelength only, metric and DH (M-DH) and DH wavelength respectively; and *blue* denotes the events with no detectable type II radio emission. Panels (c,f) show the percentage of events with enhanced type II radio bursts in each statistical bin corresponding to the left panels. The *cyan* and *magenta arrows* indicate the average and median values of the data respectively.

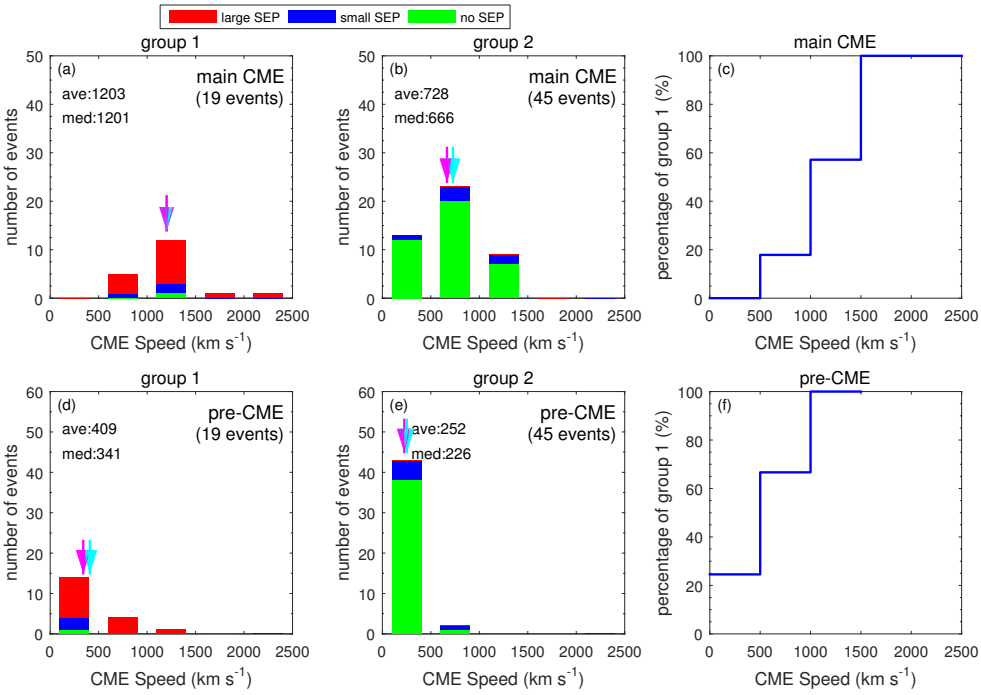

Fig. 4 Histograms of the speed of main CMEs (panels (a,b)) and preceding CMEs (panels (d,e)). The *cyan* and *magenta arrows* indicate the average and median values respectively. The *red*, *blue* and *green* colors denote large, small and no SEP events respectively. Panels (c,f) present the percentage of events that have enhanced type II radio bursts associated with each speed bin.

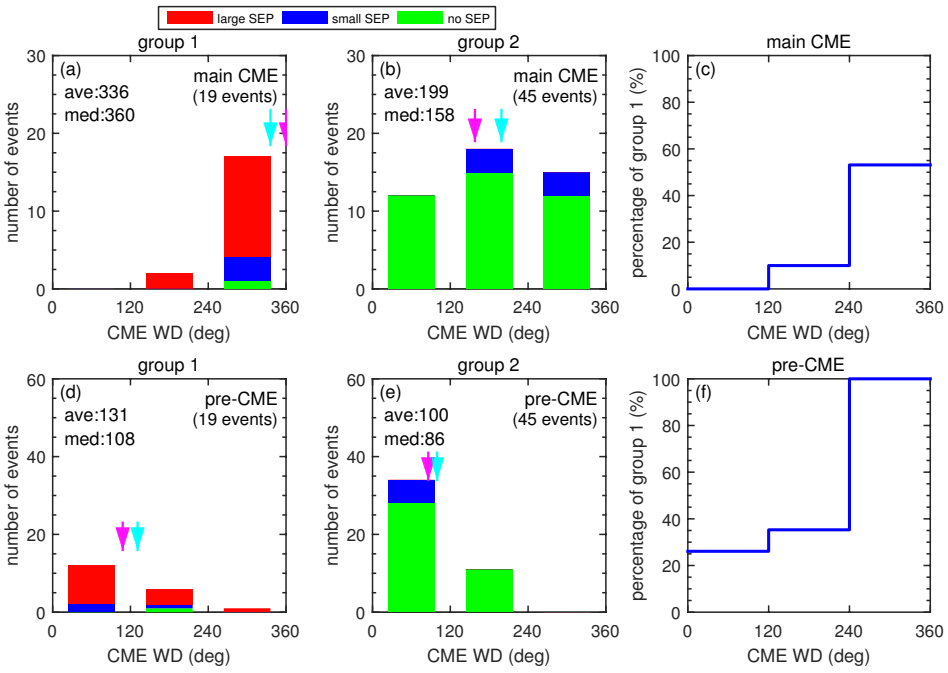

Fig. 5 Same as Fig. 4, but for the WD of CME pairs.

and preceding CME can be identified as key conditions resulting in radio enhancement?

Figure 4 shows the speed distributions of the main CMEs (top) and the preceding CMEs (bottom) for en-type-II events (group 1) and no-en-type-II events events (group 2). The speed of the main CMEs varies from 575 km s^{-1} to 2175 km s^{-1} in group 1, and 218 km s^{-1} to 1471 km s^{-1} in group 2. The difference between the average(median) speed of the main CME between two groups is distinct, i.e. 1203(1201) km s^{-1} and 728(652) km s^{-1} respectively. The speed of the main CME associated with radio enhancement is generally larger than that with no radio emission or no enhancement. However, the scatter in speed is very large, and the speed of some CMEs in group 1 can be as low as <900 km s^{-1}. Panel (c) presents the percentage of en-type-II events in each speed bin. For the main CMEs, the percentage of group 1 rises from only around 18% for v <1000 km s^{-1} to around 57% for v <1500 km s^{-1}, and to 100% for v ≥1500 km s^{-1}, which shows that the probability of type II radio burst enhancement increases rapidly with the main CME speed. For the preceding CMEs, shown in panels (d-f), the average(median) speed of group 1 is also larger than that of group 2 (409(341) vs. 252(226) km s^{-1}). The percentage of events in group 1 also shows a positive correlation with the speed of the preceding CMEs, which suggests that when two faster CMEs interact, the presence of the enhancement of type II radio bursts is more likely.

The red, blue and green bars in Figure 4 represent the interacting CME pairs associated with large SEP events ($I_{\rm p}$ ≥0.0114 cm^{-2} s^{-1} sr^{-1} MeV^{-1}), small SEP events ($I_{\rm p}$ <0.0114 cm^{-2} s^{-1} sr^{-1} MeV^{-1}) and no SEP event respectively. In group 1, about 79% (15/19) of pairs generate large SEP events and about 21% (4/19) of pairs generate small SEP events, while in group 2, none of them produce large SEP events and only about 13% (6/45) of pairs lead to small SEP events. The enhancement of type II radio bursts hereby seems to be a good discriminator between SEP-rich (or large-SEP-rich) and SEP-poor interacting CME pairs.

The CME WD in the FOV of *SOHO*/LASCO is shown in Figure 5. For the main CME (top panels), the typical WD of en-type-II events (average 336°, median 360°) is much larger than that of no-en-type-II events (average 199°, median 158°). A great majority of en-type-II main CMEs (84%, 16/19) is halo CMEs, compared to the no-en-type-II main CMEs (29%, 13/45). As shown in panel (c), the percentage of group 1 in the bin of the large WD is distinctly higher than that of the small WD. The percentage of CME pairs associated with enhanced type II radio bursts rises from only about 10% for the WD of the main CME below 240° to about 53% for WD greater than 240°, which may be attributed to the fact that there is a high proportion of halo CMEs. The preceding CMEs in group 1 have a similar distribution as those in group 2 (bottom panels): the number of events in each bin seems to de-

crease with increasing WD. The en-type-II pre-CMEs are slightly wider than the no-en-type-II ones (average: 131° vs. 100°, median: 108° vs. 86°). Here we must note that the WD from CDAW is only the projected value measured in the sky plane, which may be significantly different from the deprojected value (Shen et al. 2013a). In this study, we only compare the relative size for CME width in different groups and do not use the absolute WD value.

The mass and kinetic energy of interacting CMEs may also be important factors for type II radio enhancement and/or the occurrence of SEP events. The statistical results are shown in Figures 6 and 7.

The log mass of the main CMEs in group 1 (average 16.10, median 16.13) is typically higher than that in group 2 (15.59, 15.65), as displayed in Figure 6(a,b). From the percentage distribution of radio-enhanced events along the log mass, as shown in Figure 6(c), we find that the main CME with higher mass can more easily drive an enhanced type II radio burst than the lower mass main CME (up to about 60% with high mass). Among all interacting CME pairs listed in this study, none of the main CMEs with log mass below 15.5 can generate any SEP event or the signature of radio enhancement. The en-type-II pre-CMEs also mostly have higher mass than the no-en-type-II pre-CMEs (log mass: average 15.68 vs. 15.21, median 15.71 vs. 15.30) (Fig. 6(d,e)). The proportion of en-type-II events tends to increase almost linearly when the pre-CME mass increases, as depicted in Figure 6(f). From this figure, it is found that all SEP events (both large and small) are associated with interacting CME pairs with high mass (e.g. log mass of the main CME $>\sim$15.5, pre-CME $>\sim$14.5), no matter if there is radio enhancement or not. The possible interpretation is that a more massive CME might also be faster at driving a stronger shock to accelerate particles. It is also possible that the interaction of two massive CMEs might generate a large SEP event accompanied by an enhanced type II radio burst more easily through some mechanisms, e.g. the twin-CME scenario.

From the analysis in Figure 7 (left four panels), we can see that the kinetic energy E_k of both the main CMEs and the preceding CMEs is higher in group 1 than that in group 2, with average(median) $\log E_k$ (unit: log (erg)) 31.93(31.87) to 30.93(30.97) for main CMEs and 30.48(30.54) to 29.55(29.59) for pre-CMEs. All (large) SEP events are accelerated by the main CMEs with $\log E_k$ larger than 30.83(31.40), and by preceding CMEs with $\log E_k$ larger than 28.887(28.892). However, the no-en-type-II events can only lead to a few small SEP events with highly energetic CMEs (e.g. $\log(E_k) \geq 30$ for the main CME and ≥ 28 for the pre-CME, as displayed in the middle two panels of Fig. 7). With the kinetic energy of the main and preceding CMEs increasing, the proportion of events with type II radio enhancement also increases, as shown in the right two panels of Figure 7. This result suggests that the type II radio burst enhancement and the production of large SEPs can be generated in favor of CME interactions with high kinetic energies.

In Figure 8 (top panels), the average heliocentric distance where the leading-edge trajectories of the main CMEs intersect those of the preceding CMEs is shown. This height is typically about 11.38 R_s (median 8.67 R_s) for en-type-II events and 8.94 R_s (median 7.26 R_s) for no-en-type-II events. Since CMEs have finite thickness, the interaction of the CME pair must start before the leading-edge trajectories intersect. So, the release time of an SEP near the Sun is earlier than this leading-edge intersection. We do not find that the interaction height of the two CMEs can be used as a key factor to identify whether a pair has a type II enhancement or not. According to the CPA and WD values of the main and preceding CMEs from CDAW, we calculated and examined the overlap WD between two CMEs (see Fig. 8, bottom panels). The overlap WD of en-type-II events is typically $\sim 117^\circ$ (median 108°) and larger, compared to the no-en-type-II events $\sim 70^\circ(72^\circ)$. The percentage of en-type-II events in each bin of overlap WD tends to positively correlate with the overlap WD (Fig. 8(f)), which indicates that the interacting CME pairs having larger overlap WD (e.g. $\geq 120^\circ$) will be more likely (e.g. $\sim 60\%$ possibility) to lead to enhanced type II radio bursts. The large scatter of intersection heights and overlap WDs in SEP events in this figure also implies that the intersection height and the overlap WD of the CME pair do not seem to be deciding factors for radio enhancement or SEP generation.

3.3 SEP Intensity Dependence on the Interaction of CMEs

Since the CME interaction associated with enhanced type II radio bursts can generate SEP events more easily than that without type II or enhancement, what properties of CME interaction affect the intensities and occurrence of SEP events?

Figure 9 shows the correlation between SEP intensity I_p and intersection height H_int of the main CME leading-edge trajectory overtaking the preceding CME in the FOV of *SOHO*/LASCO. As displayed in the figure, the intensity indicates a distinctive upper limit, denoted by the dashed line, and correlates with the intersection height negatively. Also, most of the SEP events (18/24, 75%, large events 12/15, 80%) are associated with the CME pairs having

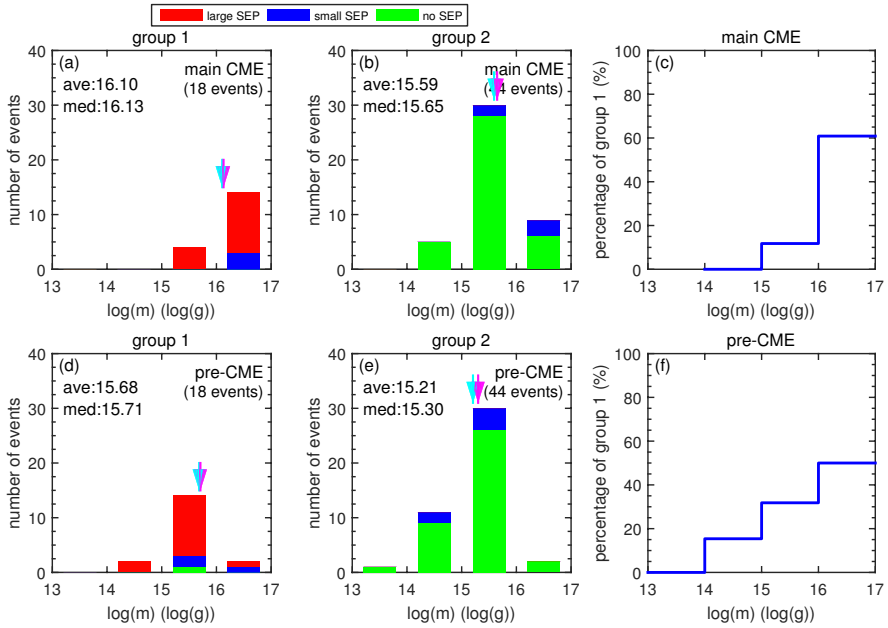

Fig. 6 Same as Fig. 4, but for the mass (m) of CME pairs.

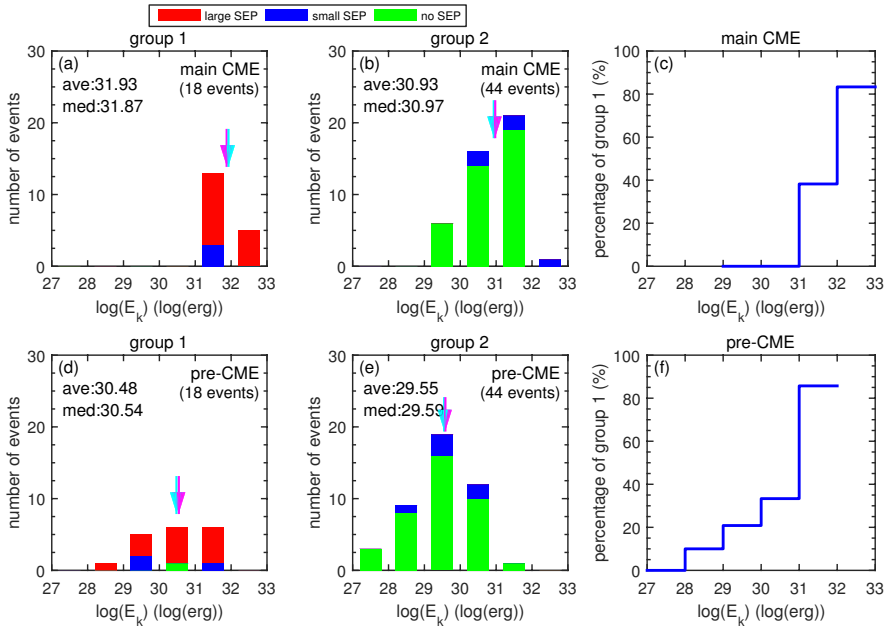

Fig. 7 Same as Fig. 4, but for the kinetic energy (E_k) of CME pairs.

interaction height smaller than $15\,R_{\rm s}$. A preceding CME captured by the main CME propagating at relatively low height tends to drive a strong shock that more likely generates a large SEP event.

Note that the actual interaction of two CMEs must start below this intersection height of leading-edge trajectories because the CMEs have a finite thickness. The acceleration and detection of SEPs is also controlled by many other aspects, such as shock strength (e.g. Kahler 1996; Shen et al. 2007), seed level (e.g. Kahler 2001; Ding et al. 2015) and magnetic field connection (e.g. Reames et al. 1996; Gopalswamy et al. 2005), so the scatter of SEP intensity as a function of intersection height is also very large.

In the process of CME interaction, the main CME may sweep partially or entirely over the body of the preceding CME. Perhaps a question one can ask is: do the relative width and overlap WD of two interacting CMEs have some effects on the generation or intensity of the SEP event? To answer this question, we tried to examine the correlations of WD and the overlap WD between the main

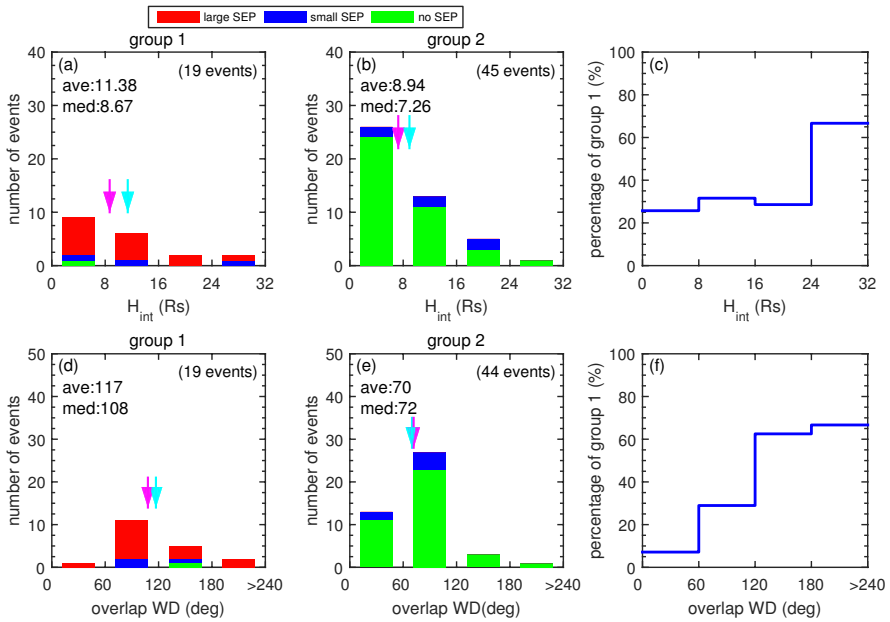

Fig. 8 Same as Fig. 4, but for the intersection height ($H_{\rm int}$) and overlap WD of CME pairs.

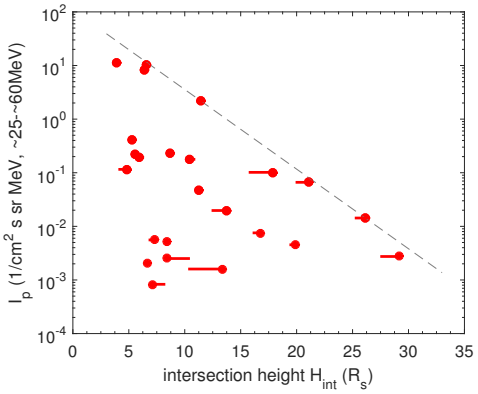

Fig. 9 The intensity ($I_{\rm p}$) of SEP events as a function of the intersection height $H_{\rm int}$ of leading-edge trajectories for two CMEs. The *dashed line* indicates the upper limit of SEP intensities.

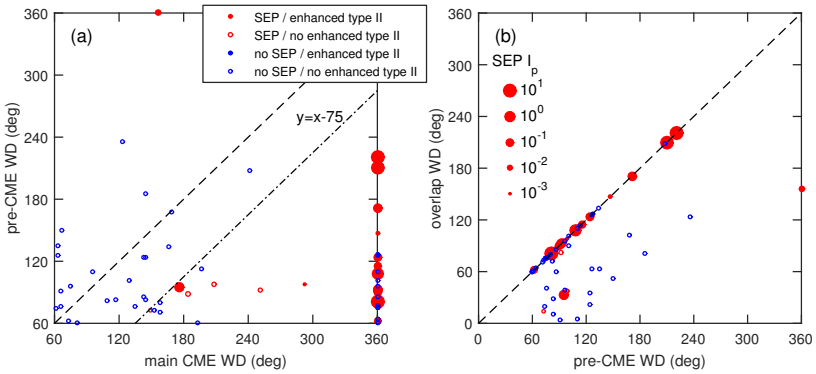

Fig. 10 (a) Preceding CME WD vs. main CME WD; (b) Overlap WD vs. preceding CME WD. Here, the *filled circles* indicate events with enhanced type II, while the *hollow circles* signify events without type II radio emissions or enhancement. *Red* corresponds to SEP-associated events, while *blue* means non-SEP events. The *dashed lines* indicate equal values, and the *dot-dashed line* shows a downward shift of 75 from the *dashed line*.

CME and pre-CME, shown in Figure 10. All SEP events but one (event 49) have been associated with main CMEs wider (even about 75° larger, indicated by dot-dashed line) than their corresponding preceding CMEs (see from panel (a)). Perhaps the fact remains that most of the large SEP events are accelerated by halo main CMEs. The overlap WD of two CMEs vs. pre-CME WD is indicated in panel (b). It is interesting to find that the overlap WD of CME pairs in almost all SEP events, except for four events, is close to the pre-CME WD, which suggests that the main CME plows completely into the preceding CME (in the sky plane). When this happens, SEP events seem to be more easily generated, especially large SEP events. Meanwhile, except for two events, all en-type-II events are also associated with this type of CME pair.

4 DISCUSSION AND CONCLUSIONS

In this paper, we focused on 64 interacting CME pairs, and investigated what properties of the main and preceding CMEs best correlate with the enhancement of a type II radio burst and whether the presence or absence of such an enhancement is related to SEP events. Various properties, such as CME speed, WD, mass, kinetic energy, intersection height and overlap WD, were examined in detail.

We approximated a comparative flux threshold of a large SEP event to the value of 0.0114(0.01) ($\mathrm{cm^{-2}\ s^{-1}\ sr^{-1}\ MeV^{-1}}$) for observations by the *STA*/*B* HET (*SOHO*/EPHIN) instrument in the energy range of $\sim$25 to $\sim$60 MeV, by which a large SEP event is defined equivalently to the event identified usually using > 10 pfu at > 10 MeV in *GOES* observations.

For events in this sample, a vast majority of SEP events, including all individual large events, occurs when the main CME overtakes the preceding CME and the accompanying type II radio burst shows enhancement. In contrast, only a few small SEP events occur for CME pairs without type II or enhancement. The en-type-II SEP events usually have a wide longitudinal distribution, compared to the no-en-type-II SEP events. In all 64 interacting CME pairs, the probability of SEP occurrence for en-type-II events is higher than that of no-en-type-II events. It suggests that the presence of type-II radio enhancement can be used as a distinct signature of whether the interaction of CME pairs can produce an SEP event or not, especially a large SEP event.

The statistical results show that the speed, WD, mass and kinetic energy of both main CMEs and preceding CMEs positively correlate with the probability of the presence of type II radio burst enhancement during CME interactions. The en-type-II events usually have higher speed, WD, mass and kinetic energy than the no-en-type-II cases. These features imply that the main and preceding CMEs are more intense and energetic, which can more easily drive a stronger shock signified by type II radio bursts and enhancement.

In our study, the intersection height and overlap WD are roughly used to quantify the extent of the interaction of two CMEs. The intersection height seems to show no distinct difference between the presence and absence of radio enhancement. However, the intensity of SEP events was found to correlate inversely with the intersection height. This result indicates that if two CMEs interact in the lower corona during their propagation, due to perhaps a higher speed of the main CME, they can produce larger SEP events more easily. The overlap WD of en-type-II events is obviously larger than that of no-en-type-II events. The portion of en-type-II events increases when the overlap WD becomes larger. All but one en-type-II event are associated with the main CMEs having a wider WD than that of the preceding CMEs. However, it must be pointed out that most main CMEs with radio enhancement are halos. The result also shows that most SEP events (20/24) are accelerated by the main CMEs widely overtaking the preceding CMEs or with the largest overlap in the sky plane. A possible interpretation may be that when a fast and wide CME widely sweeps up a narrower and slower preceding CME, particle acceleration of the shock can become more efficient either because of the enhanced seed particles injected into the shock surface or because of the trapping and acceleration of energetic particles in the closed flux loop of pre-CMEs intersecting with the shock surface. We therefore suggest that if an energetic fast and wide CME overtakes its preceding CME fully at a low height, with the presence of enhanced type II radio emissions, then the CME pair generally can generate a high intensity SEP event. These results can help us to further understand the relationship between CME interaction and large SEP events, and the mechanism of large SEP events that are triggered by CME-driven shock.

Acknowledgements We acknowledge the use of the online CME catalog CDAW (*cdaw.gsfc.nasa.gov /CME_list*), *SOHO*, *STEREO*, *GOES*, *Wind*/WAVES and ground radio station (Learmonth, Palehua, San-vito, Sagamore-hill) data provided through the indicated websites. This work is supported at NUIST by the National Natural Science Foundation of China (NSFC) (Grant Nos. U1731105 and 41304150), the Natural Science Foundation of Jiangsu Province of China (No. BK20171456), and sponsored also by the Qing Lan Project of Jiangsu Province for L.G. Ding (2016). L. Feng is supported by NSFC (Grant Nos.

11522328, 11473070 and 11427803), and also acknowledges the Youth Innovation Promotion Association and the specialized research fund from the State Key Laboratory of Space Weather for financial support.

References

Bougeret, J.-L., Kaiser, M. L., Kellogg, P. J., et al. 1995, Space Sci. Rev., 71, 231

Bougeret, J. L., Goetz, K., Kaiser, M. L., et al. 2008, Space Sci. Rev., 136, 487

Brueckner, G. E., Howard, R. A., Koomen, M. J., et al. 1995, Sol. Phys., 162, 357

Cane, H. V., & Richardson, I. G. 2003, Geophys. Res. Lett., 30, 2233

Cho, K.-S., Bong, S.-C., Kim, Y.-H., et al. 2008, A&A, 491, 873

Cliver, E. W., Kahler, S. W., & Reames, D. V. 2004, ApJ, 605, 902

Desai, M., & Giacalone, J. 2016, Living Reviews in Solar Physics, 13, 3

Ding, L., Jiang, Y., Zhao, L., & Li, G. 2013, ApJ, 763, 30

Ding, L.-G., Li, G., Dong, L.-H., et al. 2014a, Journal of Geophysical Research (Space Physics), 119, 1463

Ding, L.-G., Li, G., Jiang, Y., et al. 2014b, ApJ, 793, L35

Ding, L.-G., Li, G., Le, G.-M., Gu, B., & Cao, X.-X. 2015, ApJ, 812, 171

Ding, L.-G., Jiang, Y., & Li, G. 2016, ApJ, 818, 169

Gopalswamy, N., Yashiro, S., Kaiser, M. L., Howard, R. A., & Bougeret, J.-L. 2001, ApJ, 548, L91

Gopalswamy, N., Yashiro, S., Michałek, G., et al. 2002, ApJ, 572, L103

Gopalswamy, N., Yashiro, S., Michalek, G., et al. 2003, in American Institute of Physics Conference Series, 679, Solar Wind Ten, ed. M. Velli, R. Bruno, F. Malara, & B. Bucci, 608

Gopalswamy, N., Yashiro, S., Krucker, S., Stenborg, G., & Howard, R. A. 2004, Journal of Geophysical Research (Space Physics), 109, A12105

Gopalswamy, N., Aguilar-Rodriguez, E., Yashiro, S., et al. 2005, Journal of Geophysical Research (Space Physics), 110, A12S07

Gopalswamy, N., Thompson, W. T., Davila, J. M., et al. 2009, Sol. Phys., 259, 227

Howard, R. A., Moses, J. D., Vourlidas, A., et al. 2008, Space Sci. Rev., 136, 67

Kahler, S. W. 1982, ApJ, 261, 710

Kahler, S. W. 1996, in American Institute of Physics Conference Series, 374, eds. R. Ramaty, N. Mandzhavidze, & X.-M. Hua, 61

Kahler, S. W. 2001, J. Geophys. Res., 106, 20947

Kahler, S. W. 2003, Advances in Space Research, 32, 2587

Kahler, S. W. 2005, ApJ, 628, 1014

Kahler, S. W., Reames, D. V., & Burkepile, J. T. 2000, in Astronomical Society of the Pacific Conference Series, 206, High Energy Solar Physics Workshop - Anticipating Hess!, eds. R. Ramaty, & N. Mandzhavidze, 468

Kahler, S. W., & Vourlidas, A. 2014, ApJ, 784, 47

Lario, D., Aran, A., Gómez-Herrero, R., et al. 2013, ApJ, 767, 41

Le, G.-M., Li, C., & Zhang, X.-F. 2017, RAA (Research in Astronomy and Astrophysics), 17, 073

Le, G.-M., & Zhang, X.-F. 2017, RAA (Research in Astronomy and Astrophysics), 17, 123

Li, C., Tang, Y. H., Dai, Y., Fang, C., & Vial, J.-C. 2007a, A&A, 472, 283

Li, C., Tang, Y. H., Dai, Y., Zong, W. G., & Fang, C. 2007b, A&A, 461, 1115

Li, G., Moore, R., Mewaldt, R. A., Zhao, L., & Labrador, A. W. 2012, Space Sci. Rev., 171, 141

Li, Y.-F., & Ma, J. X. 2005, in American Institute of Physics Conference Series, 799, New Vistas in Dusty Plasmas, eds. L. Boufendi, M. Mikikian, & P. K. Shukla, 173

Liu, Y. D., Luhmann, J. G., Kajdič, P., et al. 2014, Nature Communications, 5, 3481

Lugaz, N., Temmer, M., Wang, Y., & Farrugia, C. J. 2017, Sol. Phys., 292, 64

Mason, G. M., Dwyer, J. R., & Mazur, J. E. 2000, ApJ, 545, L157

Mason, G. M., Mazur, J. E., & Dwyer, J. R. 1999, ApJ, 525, L133

Müller-Mellin, R., Kunow, H., Fleißner, V., et al. 1995, Sol. Phys., 162, 483

Reames, D. V. 1995, Reviews of Geophysics, 33, 585

Reames, D. V. 1999, Space Sci. Rev., 90, 413

Reames, D. V., Barbier, L. M., & Ng, C. K. 1996, ApJ, 466, 473

Richardson, I. G., Lawrence, G. R., Haggerty, D. K., Kucera, T. A., & Szabo, A. 2003, Geophys. Res. Lett., 30, 8014

Richardson, I. G., von Rosenvinge, T. T., Cane, H. V., et al. 2014, Sol. Phys., 289, 3059

Shanmugaraju, A., Prasanna Subramanian, S., Vrsnak, B., & Ibrahim, M. S. 2014, Sol. Phys., 289, 4621

Shen, C., Wang, Y., Ye, P., et al. 2007, ApJ, 670, 849

Shen, C., Wang, Y., Wang, S., et al. 2012, Nature Physics, 8, 923

Shen, C., Wang, Y., Pan, Z., et al. 2013a, Journal of Geophysical Research (Space Physics), 118, 6858

Shen, C., Li, G., Kong, X., et al. 2013b, ApJ, 763, 114

Temmer, M., Veronig, A. M., Peinhart, V., & Vršnak, B. 2014, ApJ, 785, 85

von Rosenvinge, T. T., Reames, D. V., Baker, R., et al. 2008, Space Sci. Rev., 136, 391

Wu, S.-S., & Qin, G. 2018, Journal of Geophysical Research (Space Physics), 123, 76

Zhao, M.-X., Le, G.-M., & Chi, Y.-T. 2018, RAA (Research in Astronomy and Astrophysics), 18, 074